PERFORMANCE ANALYSIS OF A HYBRID FARM (PHOTOVOLTAIC SYSTEM WIND TURBINE) CONNECTED TO THE GRID USING NINE-SWITCHES CONVERTER

Younes DRIS[1], Mohamed Choukri BENHABIB[2], Sidi Mohammed MELIANI[3], Virgil DUMBRAVA[4]

Nowadays, the production of electricity from photovoltaic systems and wind turbines is experiencing significant development. These energy sources can be installed independently or in the form of a hybrid system. In this paper, the hybrid configuration is developed using the nine-switch converter (NSC) to connect the doubly fed induction generator (DFIG) and the photovoltaic (PV) panels to supply the power grid. The fuzzy logic control (FLC) and the tip speed ratio (TSR) technique are used to control the PV system and the DFIG respectively. The studied system is simulated using MATLAB SimPowerSystem. The studied system is tested in many aspects. The tracking test to verify the maximum power point tracking (MPPT) control. Then, the quality of the produced energy is tested by fast Fourier transform (FFT) and the total harmonic distortion (THD) analysis. Next, the power losses of the NSC are computed. Finally, the obtained results are given and discussed.

Keywords: photovoltaic system; wind turbine; hybrid system; nine switch converter NSC; doubly fed induction generator DFIG; power grid; maximum power point tracking MPPT; Fuzzy logic control FLC; tip speed ratio TSR.

1. Introduction

Recently, high energy demand and attention to environmental issues have been pushing the world to use renewable energies. Among these energies, wind and photovoltaic energy are the most promising and affordable. The worldwide cumulative installed photovoltaic and wind power capacity has grown exponentially to reach 627 GW and 651 GW respectively in 2019 [1]. Although these sources are widely used separately, they combination is more cost-effective, which is called hybrid system [2]. There is many wind turbines generators used in

[1] Laboratoire d'automatique (LAT), Université de Tlemcen, Algeria, e-mail: younes.dris@univ-tlemcen.dz
[2] Manufaturing Engineering Laboratory (MELT), Université de Tlemcen, Algeria, e-mail: mohamedchoukri.benhabib@univ-tlemcen.dz
[3] Manufaturing Engineering Laboratory (MELT), Université de Tlemcen, Algeria, e-mail: sidimohammed.meliani@univ-tlemcen.dz
[4] Faculty of Power Engineering, University POLITEHNICA of Bucharest, Romania, e-mail: v_dumbrava@yahoo.com

such applications. In [3], it was concluded that the doubly fed induction generator (DFIG) is the favorite choice. The size of its converter is estimated to be around 30% of the total generator power. Due to the development of power electronic devices, several inverter topologies are employed to connect wind turbines to the power grid [4]. In [5], the direct AC/AC converter is discussed. In [6], a comparative analysis of the flying capacitor and H-bridge multilevel matrix converters is done. Despite the study shows a little difference in the fast Fourier transform (FFT) analysis, but both topologies have a good quality of energy. The downside of these inverters is the complicated control. Other topologies have a simple control as the neutral point converter (NPC) studied in [7]. This converter is used to feed a hybrid renewable energy system. The result shows that the quality of the energy produced has improved considerably, particularly with the proposed control. In [8], the back-to-back inverter is used to connect the DFIG to the grid. In [9], two back-to-back inverters are used in parallel. A selective algorithm is used to reduce the power losses and ameliorate the total harmonic distortion (THD). The high number of electronic power switches used in this inverters increases the cost of the system. Much research has done to reduce the number of power switches in the converter. A five-leg converter topology is presented in [10] with only 10 switches. It is evident from the results that this topology can be used in such applications, but its control is more complicated. Another topology has been proposed in [11] which is called the nine switch converter (NSC). As well as the reduced number of power electronics (9 switches), the control of this converter is very simple. In this paper, the NSC is used to combine the DFIG and photovoltaic (PV) panels into one farm. There are three types of configurations to connect these sources namely the DC coupling, the AC coupling, and the hybrid coupling [12]. In our work, we are interested to use the hybrid coupling, the PV panels are connected into the DC bus voltage of the NSC and the stator is connected directly into the grid. The purpose of this study is to test the performance and viability of the proposed converter in renewable energy applications. This research aims to reduce the cost of the hybrid farm and keep the control simple and efficient using the NSC.

2. System description

Unlike the induction generator (IG), the rotor windings of the DFIG are powered by the NSC. This inverter has the particularity of the reduced number of power electronics, only 9 switches and a capacitor for the DC bus. The aim of this paper is to exploit the DC bus of the NSC to connect PV panels. The boost converter is employed to connect PV panels to the NSC. The control of this converter is based on the fuzzy logic control (FLC) to extract the maximum power from PV panels. The NSC is controlled to extract the maximum power from the

wind and to keep the DC bus voltage constant at the desired value. Figure 1 shows the diagram of the proposed hybrid system (PV panels-DFIG). In this paper, the nominal power of the DFIG is 2 MW and the power of PV panels is 1 MW. The DFIG has two operating modes depending on the rotor speed. In the sub synchronous mode, the rotor absorbs the power. In this study, the power necessary to feed the rotor can be extracted from the grid or from PV panels. In the super synchronous mode, the rotor produces the power which will be injected into the grid. The DFIG stator always supplies the grid, regardless of the operating mode. In our case, the NSC is rated to support 1.6 MW included the PV power system (1 MW) and the DFIG rotor power (0.6 MW).

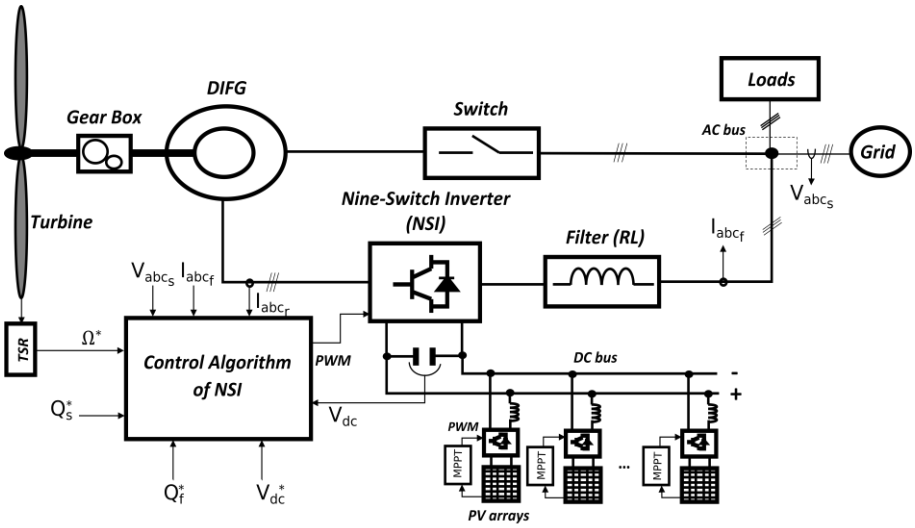

Fig. 1. Diagram of the proposed hybrid system based on PV panels and the DFIG.

3. Modelling of PV system

The sunlight captured by photovoltaic cells is directly transformed into electricity. The elementary components of photovoltaic cells are the semiconductors. A lot of studies have carried out on the PV cells modelling (model of three diodes, two diodes and single diode). In this work, the model of single diode was chosen because of its simplicity and its results are similar to those of real PV cell. According to [13], the output current of the PV panel is characterized by the following equation:

$$I = I_{ph} - I_0 \left[e^{\left(\frac{V_{pv} + R_s I}{V_t a} \right)} - 1 \right] - \frac{V_{pv} + R_s I}{R_p} \tag{1}$$

where: I_{ph} and I_0 are the current source (the photocurrent) and the diode reverse saturation current respectively. V_{pv} and V_t are the PV voltage and the thermal voltage respectively. R_s and R_p are the series resistance and the parallel resistance respectively. a is the diode ideality constant.
As it is observed from equation 1, the PV panel has non-linear characteristics. In most cases, the operating point does not correspond to the point of maximum power. To follow this point, many algorithms have been suggested [14]. In this work, the FLC is used to track the maximum power point. This MPPT can work without the need for a precise mathematical model. In [15], the comparison results show that FLC has the good efficiency and the shortest response time. The input variables are the error (E) and its variation (DE) which are expressed as following:

$$\begin{cases} E(k) = \dfrac{P_{pv}(k) - P_{pv}(k-1)}{V_{pv}(k) - V_{pv}(k-1)} \\ \Delta E(k) = E(k) - E(k-1) \end{cases} \tag{2}$$

where: P_{pv} and V_{pv} are the power and voltage of the PV respectively.
The control rules are shown in table 1[15].

Table 1

Fuzzy controller Rules [15]

E \ *ΔE*	NB	NS	ZO	PS	PB
NB	ZO	ZO	NB	NB	NB
NS	ZO	ZO	NS	NS	NS
ZO	NS	ZO	ZO	ZO	PS
PS	PS	PS	PS	ZO	ZO
PB	PB	PB	PB	ZO	ZO

where: PB (positive big), PS (positive small), ZO (zero), NS (negative small) and NB (negative big) are the five FLC levels.
The output of the FLC is the duty ratio variation ΔD, which is used to compute the duty ratio D using the following equation:

$$D(k) = D(k-1) + \Delta D(k) \tag{3}$$

4. Modelling of wind turbine based on DFIG

The energy captured by the wind turbine is given as follows:

$$P_t = \frac{1}{2}\rho\pi R^2 V_w^3 C_p(\lambda, \beta) \tag{4}$$

where: V_w is the wind speed, R is the blade radius, ρ is the air density and C_p is the performance coefficient.

The widely used expression of C_p is given as follows:

$$\begin{cases} C_p(\lambda,\beta) = c_1\left(\frac{c_2}{\lambda_i} - c_3\beta - c_4\beta^{c_5} - c_6\right)e^{\frac{-c_7}{\lambda_i}} \\ \frac{1}{\lambda_i} = \frac{1}{\lambda + c_8\beta} - \frac{c_9}{1+\beta^3} \\ \lambda = \frac{R\Omega_t}{V_v} \end{cases} \tag{5}$$

where: λ is the tip-speed ratio and β the pitch angle of the blades. c_1 to c_9 are the power coefficients (see table 8 in the appendix). Ω_{tur} is the angular speed of the wind turbine.

Theoretically, the maximum value of the C_p is approximately 59%. Due to the non-linearity of the turbine model, the MPPT control is required to extract maximum power from the wind. The model of the drive train is given by the following equation:

$$\begin{cases} J\frac{d\Omega_g}{dt} = \frac{C_{tur}}{G} - C_{em} \\ J = \frac{J_{tur}}{G^2} + J_g \end{cases} \tag{6}$$

where: J_{tur} and J_g are the inertia of the turbine and the DFIG respectively. C_{tur} and C_{em} are the turbine torque and the electromagnetic torque respectively. Ω_g is the speed of the DFIG. G is the gearbox ratio.

The electrical model of the DFIG in d-q reference is expressed as follows:

$$\begin{cases} V_{sd} = R_s I_{sd} + \frac{d\varphi_{sd}}{dt} - \omega_s\varphi_{sq} \\ V_{sq} = R_s I_{sq} + \frac{d\varphi_{sq}}{dt} + \omega_s\varphi_{sd} \\ V_{rd} = R_r I_{rd} + \frac{d\varphi_{rd}}{dt} - \omega_r\varphi_{rq} \\ V_{rq} = R_r I_{rq} + \frac{d\varphi_{rq}}{dt} + \omega_r\varphi_{rd} \end{cases} \tag{7}$$

where: I_{sd} and I_{sq} are the stator currents. I_{rd} and I_{rq} are the rotor currents. R_s and R_r are the stator and the rotor resistances respectively. φ_{sq}, φ_{sd}, φ_{rq} and φ_{rd} are the

magnetic flux of the stator and the rotor respectively. ω_s and ω_r are the angular frequency of the rotor and the stator respectively.

$$\omega_r = \omega_s - p\Omega_g \tag{8}$$

where: p is the number of pole pairs.
In the d-q reference frame, both voltages of the filter and the DC link bus are given by the following expressions:

$$\begin{cases} V_{fd} = -R_f I_{fd} - L_f \dfrac{dI_{fd}}{dt} + \omega_s L_f I_{fq} + V_{sd} \\ V_{fq} = -R_f I_{fq} - L_f \dfrac{dI_{fq}}{dt} - \omega_s L_f I_{fd} + V_{sq} \\ \dfrac{dV_{dc}}{dt} = \dfrac{1}{C_{cap}} I_{cap} \end{cases} \tag{9}$$

where: I_{fd} and I_{fq} are the currents of the RL filter. I_{cap} is the current of the capacitor C_{cap}. L_f and R_f are the inductance and the resistance of the RL filter.

5. Control of the studied system

The generator PVs (PVs + boost converter) are controlled by using the FLC. The DFIG control consists of two parts: the grid side converter (GSC) control and the rotor side converter (RSC) control. The grid angular frequency is estimated using the phase locked loop (PLL) [16]. In both parts, the oriented vector control technique is used to simplify the mathematical model of the system.

5.1. RSC control

The active and reactive power of the stator are controlled using the RSC. For easy control, the model of the DFIG is simplified. The stator voltage is considered constant and equal to the grid voltage. The stator winding resistance is neglected. The simplified model of the DFIG in synchronous frame is given as follows:

$$\begin{cases} V_{sd} = 0 \\ V_{sq} = \omega_s \varphi_{sd} \\ V_{rd} = R_r I_{rd} + \sigma L_r \dfrac{dI_{rd}}{dt} - \sigma L_r \omega_r I_{rd} \\ V_{rq} = R_r I_{rq} + \sigma L_r \dfrac{dI_{rq}}{dt} + \sigma L_r \omega_r I_{rq} - \dfrac{gMV_{sq}}{L_s} \end{cases} \tag{10}$$

where: L_s and L_r are the stator and the rotor inductance respectively. M is the mutual inductance and σ is the machine leakage coefficient.

$$\sigma = 1 - \frac{M^2}{L_s L_r} \tag{11}$$

The equations of the active and reactive power of the DFIG stator is given as follows:

$$\begin{cases} P_s = \frac{3}{2} V_{sq} I_{sq} \\ Q_s = \frac{3}{2} V_{sq} I_{sd} \end{cases} \tag{12}$$

The direct axis reference current is chosen to keep the reactive power equal to zero, while the quadrature axis reference is selected to extract the maximum power. There are many techniques to track the maximum power point [17]. In this paper, the tip speed ratio (TSR) control is used. The principle of this technique is to regulate the generator speed to maintain C_p constant regardless of the wind speed. The outer loop controls the DFIG speed while the inner loop regulates the currents of the DFIG stator. Both loops use a simple proportional integral (PI) regulator. Figure 2 shows the diagram of the RSC control.

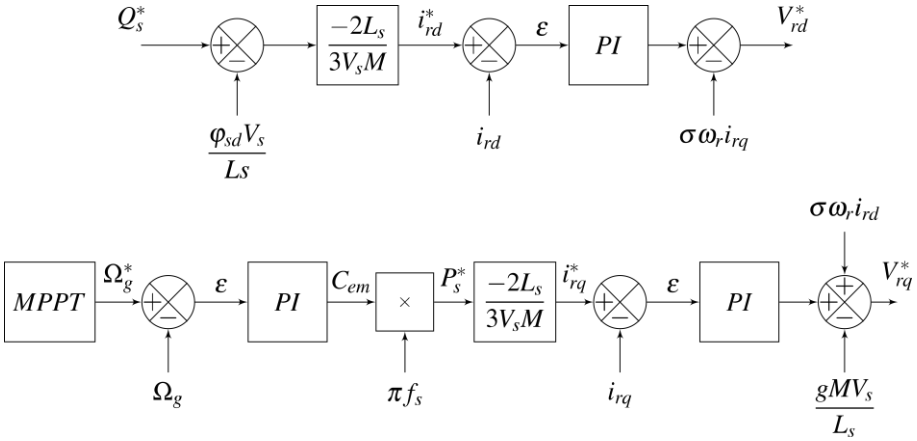

Fig. 2. Diagram of the RSC control.

5.2. GSC control

The GSC is used to control the DC bus voltage and the reactive power of the filter. Using vector control, the filter voltage equations are simplified as follows:

$$\begin{cases} V_{fd} = -R_f I_{fd} - L_f \dfrac{dI_{fd}}{dt} + \omega_s L_f I_{fq} \\ V_{fq} = -R_f I_{fq} - L_f \dfrac{dI_{fq}}{dt} - \omega_s L_f I_{fd} + V_{sq} \\ \dfrac{dV_{dc}}{dt} = \dfrac{1}{C_{cap}} I_{cap} \end{cases} \tag{13}$$

The active and reactive power of the filter is expressed as follows:

$$\begin{cases} P_f = \dfrac{3}{2} V_{sq} I_{fq} \\ Q_f = \dfrac{3}{2} V_{sq} I_{fd} \end{cases} \tag{14}$$

From the equations 14, it is obvious that the active and reactive power are decoupled. Neglecting the power losses in the NSC, the relation between the filter power P_f, the rotor power P_r, the PV generators power P_{pv} and the capacitor power P_{cap} is given as follows:

$$P_f = P_{cap} - P_r - P_{pv} \tag{15}$$

The outer loop of the GSC control is used to control the DC bus voltage and the inner loop is used to regulate the RL filter currents. The PI regulator is used in both loops. The diagram of the GSC control is illustrated in figure 3.

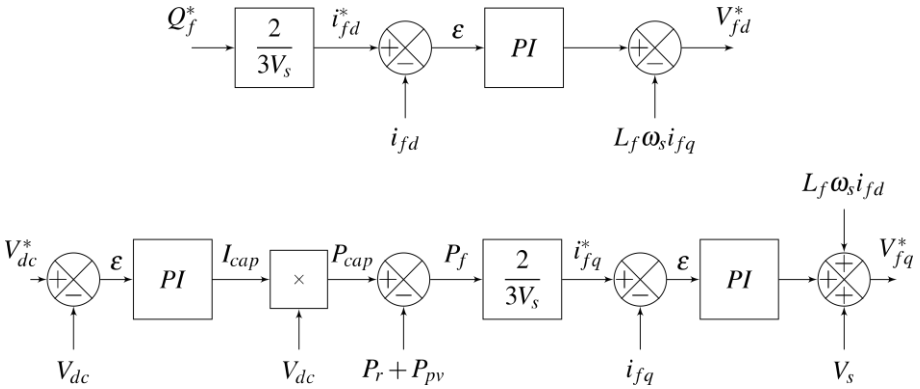

Fig. 3. Diagram of the GSC control.

6. Nine switch converter

The NSC is a bidirectional AC/AC converter with a DC link voltage connected to the top and the bottom rails [18]. The NSC has only three arms with

three switches (S_1, S_2, and S_3) on each of them. The diagram of the NSC is shown in figure 4.

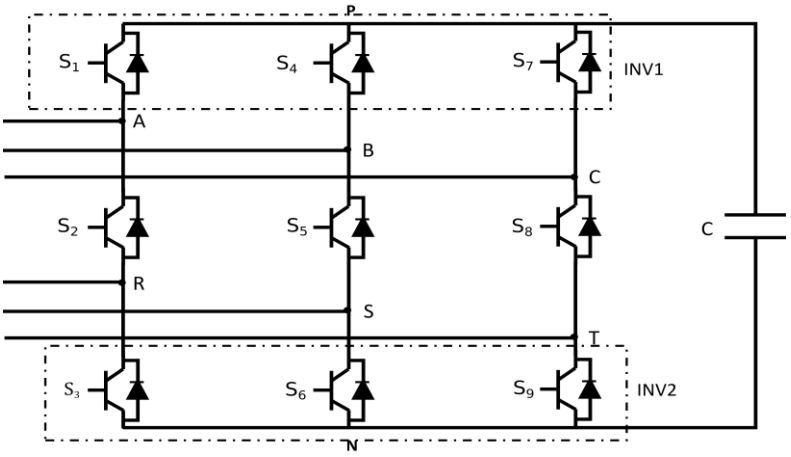

Fig. 4. Electrical diagram of the NSC.

The top switches are called INV1 and the bottom switches are called INV2, while the middle switches are used in common by INV1 and INV2. The NSC operates in constant frequency mode and variable frequency mode. In DFIG application, the variable frequency mode is considered. Table 2 shows the switching pattern design of the NSC.

Table 2

Switch states and converter voltage in one arm [18]

	S_1	S_2	S_3		V_{AN}	V_{RN}
Switch states	ON	ON	OFF	INV voltages	V_{dc}	V_{dc}
	OFF	ON	ON		0	0
	ON	OFF	ON		V_{dc}	0

It is obvious that the INV2 voltage V_{RN} must not exceed the INV1 voltage V_{AN}. In [11] the switching function is described as follows:

$$\begin{cases} S_1 + S_2 + S_3 = 2 \\ V_{AN} \geq V_{RN} \end{cases} \tag{16}$$

To satisfy this constraint, the sum of both modulation indexes of INV1 and INV2 cannot be higher than 1. There is a lot of topology used to generate the switching waveforms. In [19] the space vector pulse width modulation PWM was investigated. In [20], the discontinuous PWM scheme has been proved. In [21], an optimal PWM has been developed. In this paper, sinusoidal PWM is used because it is simpler than the previous PWM schemes and gives satisfactory results [22]. The modulation equation is given as follows:

$$\begin{cases} m_1 = \dfrac{2V_{f_{abc}}}{V_{dc}} + 0.5 \\ m_2 = \dfrac{2V_{r_{abc}}}{V_{dc}} - 0.5 \end{cases} \tag{17}$$

where: V_{fabc} and V_{rabc} are the voltage reference of the GSC and the RSC respectively. Figure 5 shows the method of generating control signals respecting the previous constraints [22]. The modulating waves m_1 and m_2 are adjusted within the half of the carrier's magnitude. Therefore, the DC bus voltage V_{dc} is considered to be twice as high as the conventional back-to-back converter.

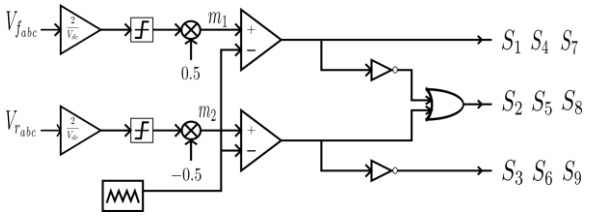

Fig. 5. Diagram of generating the PWM of the NSC.

Power losses in a switch of the NSC (Insulated-gate bipolar transistor IGBT + Diode) are divided into five types namely, conduction loss of IGBT P_{conT}, conduction loss of diode P_{conD}, turn-on loss of IGBT P_{onT}, turn-off loss of IGBT P_{offT} and reverse recovery loss of diode P_{rec} [23]. The losses model of the IGBT and the diode is given as follows:

$$\begin{cases} P_{conT} = \dfrac{1}{T}\displaystyle\int_0^T \left(V_{ce_0} + R_T i(t)\right) i(t)dt \\ P_{conD} = \dfrac{1}{T}\displaystyle\int_0^T \left(V_{F_0} + R_D i(t)\right) i(t)dt \\ P_{onT} = \dfrac{E_{on} I_{pk} f_{sw} V_{dc}}{\pi I_{nom} V_{nom}} \\ P_{offT} = \dfrac{E_{off} I_{pk} f_{sw} V_{dc}}{\pi I_{nom} V_{nom}} \\ P_{rec} = \dfrac{E_{rec} I_{pk} f_{sw} V_{dc}}{\pi I_{nom} V_{nom}} \end{cases} \tag{18}$$

where: T is the fundamental period. V_{ce0}, V_{F0} and Vnom are the IGBT bias voltage, the diode bias voltage and the nominal voltage respectively. R_T and R_D are the resistances of the IGBT and the diode respectively. $i(t)$, I_{pk} and is I_{nom} are the load current, the peak current and the nominal current respectively. E_{on}, E_{off} and E_{rec} are the energy losses. f_{sw} is the switching frequency.

7. Simulation results

The proposed hybrid farm (PVs + DFIG) presented in figure 1 is simulated by using MATLAB SimPowerSystem. The DFIG stator is connected directly to the medium or high voltage grid via a step-up transformer. To simplify the simulation, we have worked on the primary side of the transformer which depends on the DFIG stator voltage. Therefore, the hybrid farm is connected to a grid voltage of 690V/50Hz. The total power of the system is 3 MW, where, 2 MW for the DFIG and 1 MW for PV panels. The parameters of the system are listed in the appendix (tables 6, 7 and 8). The start-up procedure of the DFIG is more complicated than other AC generators. In [24], the method to connect the DFIG to the grid is described. Firstly, the GSC is enabled to charge the DC-link voltage. Next, it is necessary to wait until the speed generator achieves the required value (-30% of the synchronous speed (πf_s)). It is better to turn off the RSC so that the DFIG can be accelerated by the wind itself. To close the stator switch (break), the DFIG stator voltage and the grid voltage must be approximately equal in amplitude and have the same frequency. After the synchronizing state, the DFIG switches to the normal state operation. In this paper, the generator speed is initialized at 135 rad/s, and the initial value of the DC bus voltage is chosen to be 2200 V. The stator breaker is closed at 0.6 s, when the stator voltage and the grid voltage are similar enough. The multi-string structure is used to connect PV panels to the DC bus of the NSC. To evaluate the performance of the system, the variable weather conditions are considered. Figure 6 shows the curve of the wind speed (a), the irradiance (b) and the cell temperature (c).

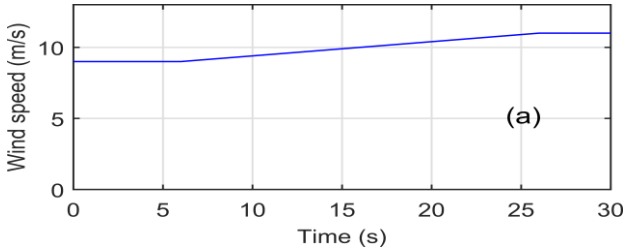

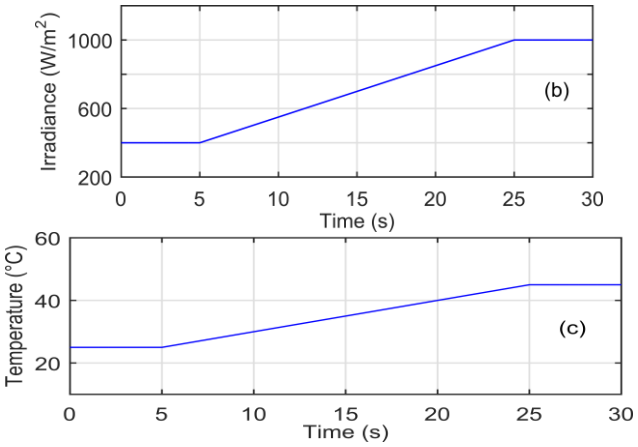

Fig. 6. Profile of weather conditions: a) wind speed, b) irradiance, c) cell temperature.

In this work, the power generated from renewable energy (injected into the grid) has a negative sign, while the power consumed from the grid has a positive sign. In this study, we have use three tests to evaluate the system.

7.1. Tracking test

The power of PV panels is presented in figure 7.

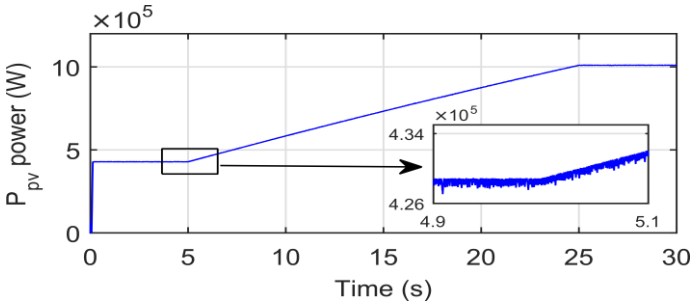

Fig. 7. Total power of PV panels.

It is observed that the FLC algorithm has a satisfactory result in terms of maximum power control regardless of changing weather conditions. In the wind turbine system, the TSR technique is used to track the maximum power point. Figure 8 shows the C_p coefficient, which varies around its maximum value ($0.441 \leq C_p \leq 0.442$).

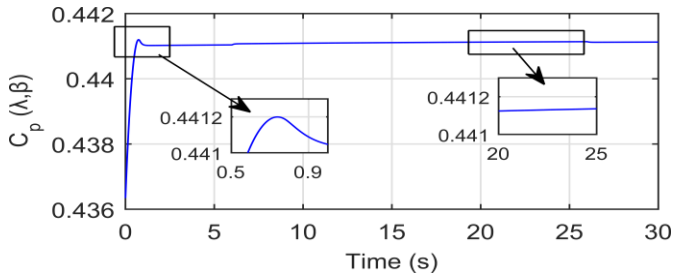

Fig. 8. C_p coefficient under variable wind.

In figure 9, it is shown that the DFIG tracks the optimal speed. Therefore, the generator produces maximum power.

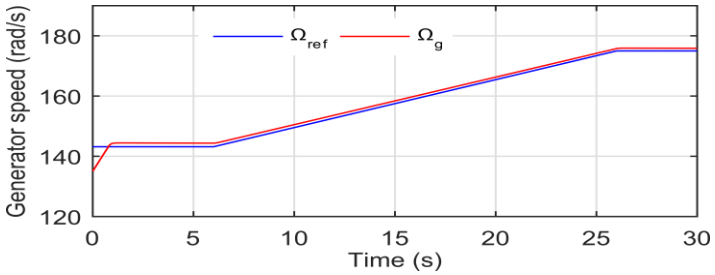

Fig. 9. Optimal and measured generator speed.

Figure 10 displays the power exchanged between the grid and the proposed system. The stator of the DFIG always produces power when the generator speed is in the range of (± 30%) of the synchronous speed. The rotor of the DFIG consumes power in the sub synchronous mode ($\Omega_g < \pi f_s$) and produces power in the super synchronous mode ($\Omega_g > \pi f_s$). In this paper, the reactive power reference Q_s is set to zero.

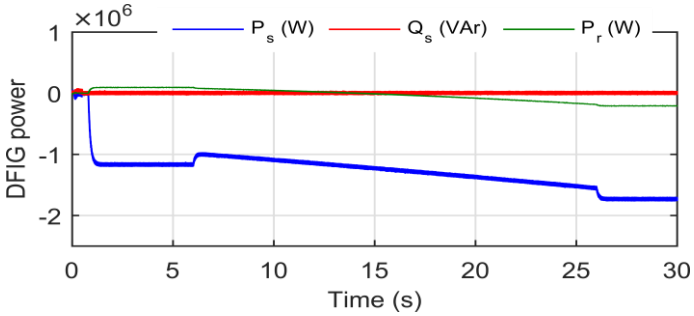

Fig. 10. Active and reactive power of the DFIG.

In the figure 11, the DC bus voltage is stabilized at the desired reference within 0.3 s and the overshoot is less than 10 V.

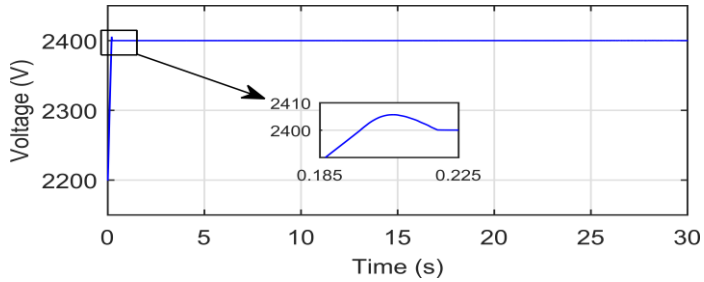

Fig. 11. DC bus Voltage of the NSC.

The control of the proposed system is simple, but it is very satisfactory in term of tracking. Both sources (PV and DFIG) produce the maximum power.

7.2. Energy produced quality test

This part is dedicated to verifying the quality of the energy produced by the proposed system. Figure 12 shows that the stator current frequency is independent of the wind speed variation.

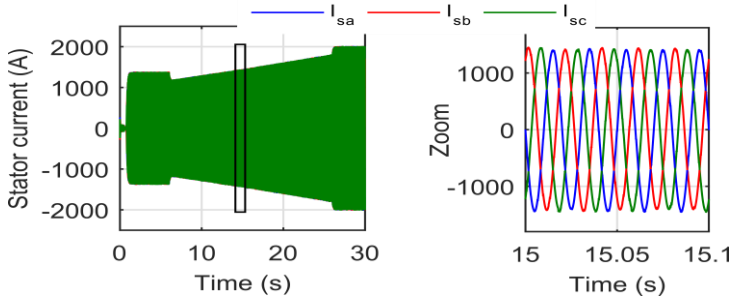

Fig. 12. Three phase stator currents.

In figure 13, it is observed that the rotor current frequency varies according to the wind speed. As we know, the production of energy from renewable sources is discontinuous. In this paper, the quality of the energy produced by this hybrid farm is tested and studied according to three cases depending on the weather conditions.

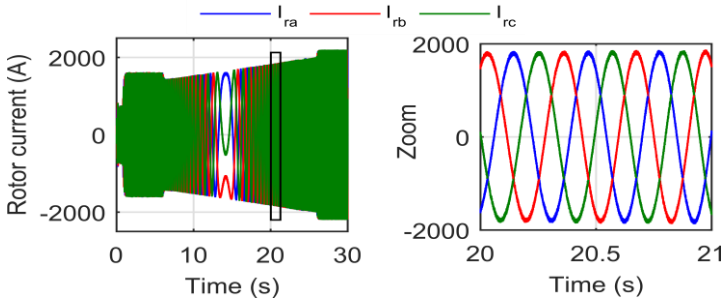

Fig. 13. Three phase rotor currents.

- **Case 1**:

Both sources produce energy, we used the same weather profiles previously used. Table 3 shows the FFT and the THD results of the total current produced at the point of common coupling (PCC).

Table 3

Analysis of the current produced by the wind turbine

Sub synchronous mode G=400 W/m^2						Super synchronous mode G=1000 W/m^2				
Current (A)	Peak		RMS			Peak		RMS		
	1712		1211			3342		2363		
Harmonics (%)	H_3	H_5	H_7	H_9	H_{11}	H_3	H_5	H_7	H_9	H_{11}
	0.01	0.04	0.05	0.03	0.02	0.04	0.4	0.35	0.01	0.06
THD (%)	1.20					0.95				

- **Case 2**:

In this case, we suppose that the PV system is disable. Table 4 shows the FFT and the THD results of the total current produced by the DFIG.

Table 4

Analysis of the current produced by the wind turbine

Sub synchronous mode						Super synchronous mode				
Current (A)	Peak		RMS			Peak		RMS		
	1217		855.9			2187		1547		
Harmonics (%)	H_3	H_5	H_7	H_9	H_{11}	H_3	H_5	H_7	H_9	H_{11}
	0	0.06	0.04	0.01	0.03	0.01	0.04	0.03	0.01	0.01
THD (%)	1.67					1.14				

- **Case 3**:

In the third case, the wind turbine system is disable. The test has done in both high and low irradiance. Table 5 shows the FFT and the THD results of the total current produced by the PV system.

Table 5

Analysis of the current produced by the wind turbine

G=400 W/m^2						G=1000 W/m^2				
Current (A)	Peak		RMS			Peak		RMS		
	497.6		351.8			1161		820.7		
Harmonics (%)	H_3	H_5	H_7	H_9	H_{11}	H_3	H_5	H_7	H_9	H_{11}
	0.01	0.04	0.01	0.01	0.02	0.05	0.03	0.03	0.01	0.01
THD (%)	2.13					1.37				

In all cases the THD is less than 5% and the individual odd harmonics from 3 to 11 are less than 4%. According to [25], these results are acceptable for grid connection system. The result shows that the proposed hybrid system can produce high quality of energy regardless the change of weather conditions.

7.3. Power losses test

In this section, the average power losses are calculated. In this test, the 5SNA2000K452300 data-sheet is used to calculate the power losses. We have

made many tests by varying the power factor (PF) and the modulation index m. We have chosen the worst case where the power losses are at their maximum (PF=1 and m=0.5). Figure 14 shows the power losses of the NSC regarding the total rating of the NSC.

8. Conclusions

In this paper, a proposed hybrid system (PVs + DFIG) connected to the grid using the NSC was studied. This structure has reduced the number of power electronics used in the conventional hybrid farm. The control of the NSC is not complicated, a simple logic circuit was used to generate the middle gates signal of the NSC. The FLC algorithm and the TSR technique are used to extract the maximum power from PV panels and the DFIG respectively. The validity of this structure is confirmed using the SimPower system. Simulation results show the efficiency of the proposed system in term of control and the produced energy quality. Using the NSC minimize the number of the power electronic switches, but connecting the photovoltaic panels to the DC link leads to increase the size of the semiconductor switches. The power losses of the NSC converter are important due to high DC bus voltage and the high size of the semiconductor switches used.

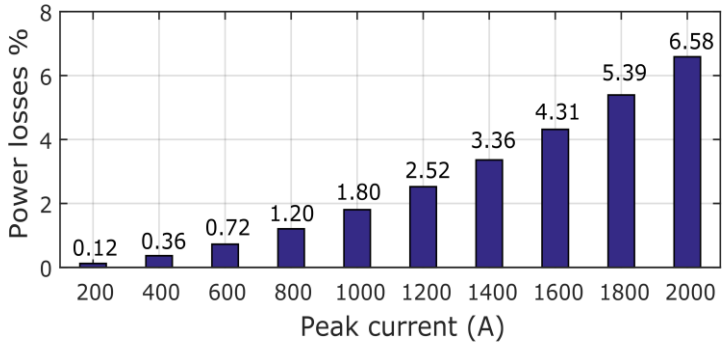

Fig. 14. Power losses of the NSC.

9. Appendix

Table 6

Photovoltaic panel parameters [26]

Parameter	Value	Unit
I_{mp}	7.84	A
V_{mp}	29.32	V
Cells N_s	60	-

Table 7

Wind turbine parameters [9]

Parameter	Value	Unit
P_s	2.0	MW
R_s	2.6	mΩ
R_r	2.9	mΩ
L_s	2.587	mH
L_r	2.587	mH
M	2.5	mH
L_f	1	mH
R_f	0.01	Ω
C_{cap}	3.8	mF
J	729	$Kg.m^2$

Table 8

C_p variables [27]

c_1	c_2	c_3	c_4	c_5	c_6	c_7	c_8	c_9
0.73	151	0.58	0.002	2.14	13.2	18.4	-0.02	-0.003

R E F E R E N C E S

[1]. REN21, Renewables 2020 global status report, https://www.ren21.net/gsr-2020/ (accessed 29 December 2020).

[2]. *R. Al Badwawi, M. Abusara and T. Mallick*, A review of hybrid solar PV and wind energy system, Smart science, **3**(2015), No. 3, 127-138 (DOI 10.1080/23080477.2015.11665647).

[3]. *H. T. Jadhav and R. Roy*, A comprehensive review on the grid integration of doubly fed induction generator, International journal of electrical power & energy systems, **49**(2013), 8-18 (DOI 10.1016/j.ijepes.2012.11.020).

[4]. *K. Ma*, Power electronics for the next generation wind turbine system, Springer, **5**(2015).

[5]. *A. Chemidi, S. M. Meliani and M. C. Benhabib*, Performance analysis of DFIG wind power system fed by matrix converter, Electrotehnica, electronica, automatica, **63**(2015), No. 1,78.

[6]. *G. P. R. Reddy, J. C. Sekhar, B. Naresh and M. V. Kumar*, Comparative analysis of flying capacitor and H-bridge multilevel matrix converters for DFIG based wind energy conversion system, (eds) Emerging Trends in Electrical, Communications, and information technologies, Lecture notes in electrical engineering, Springer, **49**(2013), 309-320 (DOI 10.1007/978-981-13-8942-9_26).

[7]. *B. Belabbas, M. Denai, and T. Allaoui*, A hierarchical control scheme to improve the stability and energy quality of a hybrid wind/photovoltaic system connected to the electricity grid, UNIVERSITY POLITEHNICA OF BUCHAREST SCIENTIFIC BULLETIN SERIES C-ELECTRICAL ENGINEERING AND COMPUTER SCIENCE, **82**(2020), No. 2, 307-323.

[8]. *M. Q. Duong, A. Dolara, F. Grimaccia, S. Leva, M. Mussetta and G. Sava*, Fault ridethrough capability and damping improvement In DFIG, UNIVERSITY POLITEHNICA OF BUCHAREST SCIENTIFIC BULLETIN SERIES C−ELECTRICAL ENGINEERING AND COMPUTER SCIENCE, **78**(2016), No. 3, 241-252.

[9]. *Y. Dris, M. C. Benhabib and S. M. Meliani*, Selective control approach for DFIG powered by parallel inverters, In the international conference in artificial intelligence in renewable energetic systems, Springer, **102**(2019), 684-692 (DOI 10.1007/978-3-030-37207-1_74).

[10]. *M. Shahbazi P. Poure S. Saadate and M. R. Zolghadri*, Five-leg converter topology for wind energy conversion system with doubly fed induction generator, Renewable energy, **36**(2011), No. 11, 3187-3194 (DOI 10.1016/j.renene.2011.03.014).

[11]. *N. P. Soe, D. M. Vilathgamuwa and K. S. Low*, Doubly Fed Induction Generator for wind energy generation using nine-switch power converter, In IECON 2011-37th annual conference of the IEEE industrial electronics society, (2011), 3608-3613 (DOI 10.1109/IECON.2011.6119895).

[12]. *M. D. Al-Falahi, S. D. G. Jayasinghe and H. Enshaei*, A review on recent size optimization methodologies for standalone solar and wind hybrid renewable energy system, Energy conversion and management, **143**(2009), 252-274 (DOI 10.1016/j.enconman.2017.04.019).

[13]. *Y. Dris, S. M. Meliani and M. C. Benhabib*, Study and simulation of a photovoltaic system connected to the three-phase electricity network, 2018 6th International conference on control engineering & information technology (CEIT), Istanbul, Turkey, 1-5 (DOI 10.1109/CEIT.2018.8751804).

[14]. *T. Esram and P. L. Chapman*, Comparison of photovoltaic array maximum power point tracking techniques, IEEE transactions on energy conversion, **22**(2007), No. 2, 439-449 (DOI 10.1109/TEC.2006.874230).

[15]. *B. Bendib, H. Belmili, F. Krim*, A survey of the most used MPPT methods: Conventional and advanced algorithms applied for photovoltaic systems, Renewable and sustainable energy reviews, **45**(2015), 637-648 (DOI 10.1016/j.rser.2015.02.009).

[16]. *M.C. Benhabib*, A contribution l'étude des différentes topologies et commandes des filtres actifs parallèles structure tension : Modélisation, simulation et validation expérimentale de la commande, Unpublished PhD thesis, Henri Poincaré university, France, (2004).

[17]. *M. A. Abdullah, A. H. M. Yatim, C. W. Tan and R. Saidur*, A review of maximum power point tracking algorithms for wind energy systems, Renewable and sustainable energy reviews, **16**(2012), No. 5, 3220-3227 (DOI 10.1109/ECCE.2012.6342546).

[18]. *C. Liu, B. Wu, N. R. Zargari, D. Xu and J. Wang*, A novel three-phase three-leg AC/AC converter using nine IGBTs, IEEE transactions on power electronics, (2009), 1151-1160 (DOI 10.1109/TPEL.2008.2004038).

[19]. *K. Aganah, S. Karugaba and O. Ojo*, Space vector and carrier-based PWM modulation schemes for maximum utilization of voltage sources of a nine-switch converter, In 2012 IEEE energy conversion congress and exposition (ECCE), (2012), 2521-2528 (DOI 10.1109/ECCE.2012.6342546).

[20]. *M. A. Abbache, B. Tabbache and A. Kheloui*, Direct torque control of nine switches inverter dual induction motors, In 22nd mediterranean conference on control and automation, (2014), 810-815 (DOI 10.1109/MED.2014.6961473).

[21]. *F. Gao, L. Zhang, D. Li, P. C. Loh, Y. Tang and H. Gao*, Optimal pulsewidth modulation of nine-switch converter, IEEE transactions on power electronics, **25**(2010), No. 9, 2331-2343 (DOI 10.1109/TPEL.2010.2047733).

[22]. *T. Kominami and Y. Fujimoto*, A novel nine-switch inverter for independent control of two three-phase loads, In 2007 IEEE industry applications annual meeting, (2007), 2346-2350 (DOI 10.1109/07IAS.2007.354).

[23]. *M. H. Bierhoff and F. W. Fuchs*, Semiconductor losses in voltage source and current source IGBT converters based on analytical derivation, In 2004 IEEE 35th annual power electronics specialists conference, 4(2004), 2836-2842 (DOI 10.1109/PESC.2004.1355283).

[24]. *A. G. Abo-Khalil*, Synchronization of DFIG output voltage to utility grid in wind power system, Renewable energy, **44**(2012), 193-198 (DOI 10.1016/j.renene.2012.01.009).

[25]. *F. Blaabjerg and K. Ma*, Renewable energy system with wind power, Power electronics in renewable energy systems and smart grid: technology and applications, (2019), 315-345 (DOI 10.1002/9781119515661.ch6).

[26]. *Y. Dris, V. Dumbrava, M. C. Benhabib and S. M. Meliani*, Super twisting control for a photovoltaic grid connected system with filtering function, In 2020 55th international universities power engineering conference (UPEC), IEEE, (2020), 1-6 (DOI 10.1109/UPEC49904.2020.9209850).

[27]. *F. Fuchs and A. Mertens*, Dynamic modelling of a 2 MW DFIG wind turbine for converter issues: Part 1, In 2012 15th International power electronics and motion control conference (EPE/PEMC), (2012), DS2d-5 (DOI 10.1109/EPEPEMC.2012.6397308).